Two-step photon absorption in InAs/GaAs quantum-dot superlattice solar cells

Kada, T. ; Asahi, S. ; Kaizu, T. ; Harada, Y. ; Kita, T. ; Tamaki, R. ; Okada, Y. ; Miyano, K.

(Citation)
Physical Review B,91(20):201303-201303

(Issue Date)
2015-05-18

(Resource Type)
journal article

(Version)
Version of Record

PHYSICAL REVIEW B **91**, 201303(R) (2015)

Two-step photon absorption in InAs/GaAs quantum-dot superlattice solar cells

T. Kada, S. Asahi, T. Kaizu, Y. Harada, and T. Kita
Department of Electrical and Electronic Engineering, Graduate School of Engineering, Kobe University, 1-1 Rokkodai, Nada, Kobe 657-8501, Japan

R. Tamaki, Y. Okada, and K. Miyano
Research Center for Advanced Science and Technology (RCAST), The University of Tokyo, 4-6-1 Komaba, Meguro-ku, Tokyo 153-8904, Japan

(Received 12 September 2014; revised manuscript received 18 March 2015; published 18 May 2015)

We studied the two-step photon absorption (TSPA) process in InAs/GaAs quantum-dot superlattice (QDSL) solar cells. TSPA of subband-gap photons efficiently occurs when electrons are pumped from the valence band to the states above the inhomogeneously distributed fundamental states of QDSLs. The photoluminescence (PL)-excitation spectrum demonstrates an absorption edge attributed to the higher excited states of the QDSLs in between the InAs wetting layer states and the fundamental states of QDSLs. When the absorption edge of the excited state was resonantly excited, the superlinear excitation power dependence of the PL intensity demonstrated that the electron and hole created by the interband transition separately relax into QDSLs. Furthermore, time-resolved PL measurements demonstrated that the electron lifetime is extended by thereby inhibiting recombination with holes, enhancing the second subband-gap absorption.

DOI: 10.1103/PhysRevB.91.201303 PACS number(s): 72.40.+w, 78.67.Hc, 88.40.fh

In the face of increasing demand for renewable energy sources to permit our safe and secure ways of life to continue, high-efficiency photovoltaics using *p-i-n* semiconductor solar cells (SCs) are very promising for generating electrical power by converting solar radiation. The conversion efficiency of a single-junction SC is limited by several unavoidable losses, such as transmission loss, thermalization loss, Carnot loss, Boltzmann loss, and emission loss [1]. The maximum conversion efficiency is thereby restrained to be approximately 30% [2]. Here, a major loss comes from transmission loss for photons with energy less than the band-gap energy of a SC. The key concept in breaking through the efficiency limit is an energy conversion covering the broad solar radiation spectrum. This can be achieved by multicolor absorption in a multi-energy gap system. Multijunction SCs comprising a series connection of junctions with different band-gap energies are one of the promising structures that accomplish the highest energy conversion efficiency [3]. Recently, the intermediate-band (IB) SC [4] with an additional parallel diode connection has attracted strong interest because of its more robust operation under a solar spectral variation in comparison to a multijunction SC [5].

Based on theoretical predictions, IBSCs are expected to realize extremely high conversion efficiency: greater than 60% under the maximum concentration and 48.2% under one-sun irradiation [6]. The IBSC with a single IB provides two additional subband-gap absorptions: valence band (VB) → IB and IB → conduction band (CB), together with the interband absorption from VB to CB. These additional transitions produce extra photocurrent without degrading the photovoltage when electrons in the IB are optically pumped out to the CB [7,8]. Since the series-connected electron pumping by way of the IB occurs under a current-matched condition, the optical transition strength between the IB and CB should be almost the same as that between the VB and IB, which generally relates to the oscillator strength and the electron density in the IB [9,10]. To enhance the second optical transition (IB → CB) for a photon flux illuminating a SC surface, zero-dimensional systems such as quantum dots (QDs) have been investigated [11,12]. Despite the use of stacked QDs for IBSC being strongly anticipated as reviewed in Refs. [4] and [8], the key physics practically realizing efficient two-step photocurrent generation has been unclear. So far, a superlattice (SL) structure has been expected to form minibands playing the role of the IB. In this work, we focus on a new role of SL in two-step photocurrent generation; efficient two-step process can be accomplished by extending electron lifetime in InAs/GaAs QDSLs. A long carrier lifetime is, of course, preferable for the second photoexcitation, as it enhances the chance of photoexcitation of electrons in the IB [13]. We studied the two-step photon absorption (TSPA) process via quantized states formed in IBSCs, including a SL structure of InAs/GaAs QDs. We carried out photoluminescence (PL) and its excitation (PLE) measurements, as well as the external quantum efficiency (EQE) measurements under two-color photoexcitation for VB → IB and IB → CB. We found that TSPA efficiently occurs when electrons are pumped into an energy level located above the inhomogeneously distributed fundamental states of QDSLs. In addition, we conducted the excitation power dependence of the PL intensity and time-resolved PL measurements to study separate electron and hole energy relaxation.

An IBSC structure was fabricated on the n^+-GaAs(001) substrate using solid-source molecular beam epitaxy. An InAs/GaAs QDSL was included in the intrinsic layer. An undoped nine-layer stacked InAs/GaAs QD was formed at 480 °C on undoped-GaAs/n-GaAs(Si: 5×10^{17} cm^{-3})/n^+-GaAs(Si: 1×10^{18} cm^{-3}) grown at 550 °C. Nominal thickness of InAs was 2.0 monolayers (ML) for the first QD layer and 1.4 ML for the stacked layers in order to prevent increasing the lateral size [14]. The beam-equivalent pressure of the As_2 flux was 1.3×10^{-3} Pa. Nominal GaAs spacer layer thickness was 4 nm, which is thin enough to couple the electronic states along the stacking direction and forms a miniband [14,15]. Then, a p^+-GaAs(Be: 1×10^{19} cm^{-3})/p-GaAs(Be: 2×10^{18} cm^{-3}) layer was grown on the top of the SC structure. Metal contacts

on the top and the bottom surface were Au/Au-Zn and In, respectively. The in-plane QD density and the total thickness of the QDSL was approximately 1×10^{10} QDs/cm^2 and 38 nm, respectively. The thickness of the intrinsic layer in the IBSC structure was 2000 nm. The built-in electric field applied to the QDSLs was expected to be 7 kV/cm, which is low enough to prevent electric-field induced carrier escape [16,17]. Here, the fundamental state does not form a miniband at temperatures less than approximately 20 K because the homogeneous linewidth producing the electronic coupling is smaller than the inhomogeneous distribution of the fundamental energy states along the stacking direction [14,16].

Photocurrent measurements were carried out at 20 and 300 K. The excitation light source used was a tungsten halogen lamp passed through a 140-mm monochromator and chopped by an optical chopper ($f = 800$ Hz). The excitation power density depending on the wavelength was 6.82–16.7 μW/cm^2, which was much smaller than that of the one-sun solar irradiance. The photocurrent was detected by a lock-in amplifier synchronized with the optical chopper. The measurements were conducted under short-circuit condition without applying any external bias voltage. Here, the EQE was defined as an efficiency of the photocurrent production under the monochromatic excitation. The EQE spectrum was obtained by the number of electrons collected as the photocurrent normalized by the incident photon flux at each wavelength.

TSPA was demonstrated by measuring a change in the EQE signal amplitude under two-color excitation using two light sources [18–22]. The primary light source, a monochromated tungsten halogen lamp, excited electrons from the VB into the IB. A second infrared (IR) light source in this experiment pumped electrons accumulated in the IB to the CB. The IR light source used here was a pulsed laser light with a photon energy of 0.30 eV and repetition rate of 200 kHz. The excitation intensity was 6.5×10^{18} photons/(cm^2 s), which is roughly equivalent to 60 times the solar irradiance in the 0.4–1.0 eV range. The photon energy of 0.30 eV was chosen to be slightly greater than the thermal activation energy of excitons in QDSLs (0.26 eV). The thermal activation energy of the confined excitons was examined by means of the temperature dependence of the PL intensity of the fundamental transition of QDSLs. ΔEQE is defined as the change in the EQE signal amplitude under the IR irradiation obtained by a lock-in amplifier synchronized with an optical chopper ($f \sim 1.8$ kHz) modulating the IR pulse trains [21].

PL and PLE were measured at 9 K. For the excitation, we used a superluminescent light source. The excitation power density depends on the wavelength was 2.02–2.88 mW/cm^2. For example, the power density at 940 nm was 2.51 mW/cm^2 and the photon-flux density was 1.19×10^{16} photons/(cm^2 s). The PLE spectrum was obtained by the PL intensity normalized by the photon flux at each wavelength. The PL signal was dispersed by a 140-mm single monochromator and detected by a deep-thermoelectric-cooled InGaAs diode array. The excitation power dependence of PL under weak illumination was also measured at 9 K while using light-emitting diodes with peak wavelengths of 940, 850, and 780 nm. Here, the excitation power densities were ~1–1000 μW/cm^2. In addition, the time-resolved PL measurements were performed at 4 K by using a near-infrared streak camera system with a temporal resolution of 20 ps. The light source used was a mode-locked Ti:sapphire pulse laser with wavelengths of 900 and 800 nm. The pulse duration was 130 fs, and the repetition rate was 80 MHz.

Figure 1(a) shows EQE spectra obtained at different temperatures. The absorption edge of the EQE spectrum at 20 K shifts according to the temperature dependence of the GaAs band gap and indicates a sharp edge. Figure 1(b) displays EQE spectra in the subband-gap region. Here, the horizontal axis is the difference between the photon energy and the GaAs band edge ($E_g = 1.52$ eV at 20 K and 1.42 eV at 300 K). EQE at 300 K is higher than at 20 K and shows a tail structure continuously extending toward the QDSL states. This can be dominantly attributed to thermally excited electrons from the InAs wetting-layer (WL) states [23]. In other words, electrons are effectively accumulated in the IB at 20 K, which is suitable for studying TSPA in an IBSC.

A typical ΔEQE spectrum measured at 9 K is shown in Fig. 2(a). The signal amplitude of ΔEQE is relatively

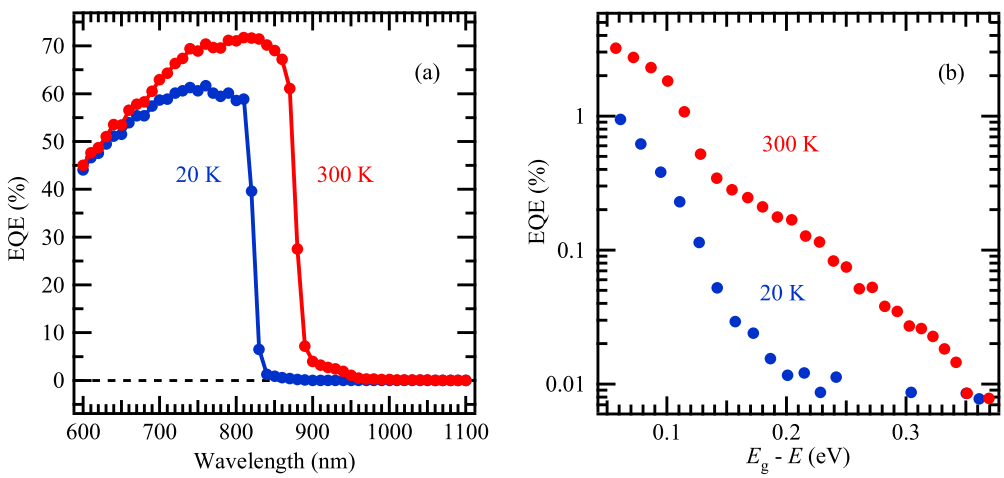

FIG. 1. (Color online) EQE spectra measured at 20 and 300 K, (a) entire spectra, and (b) magnified plots in the subband-gap region. The horizontal axis is the difference between the photon energy and the GaAs band edge ($E_g = 1.52$ eV at 20 K and 1.42 eV at 300 K).

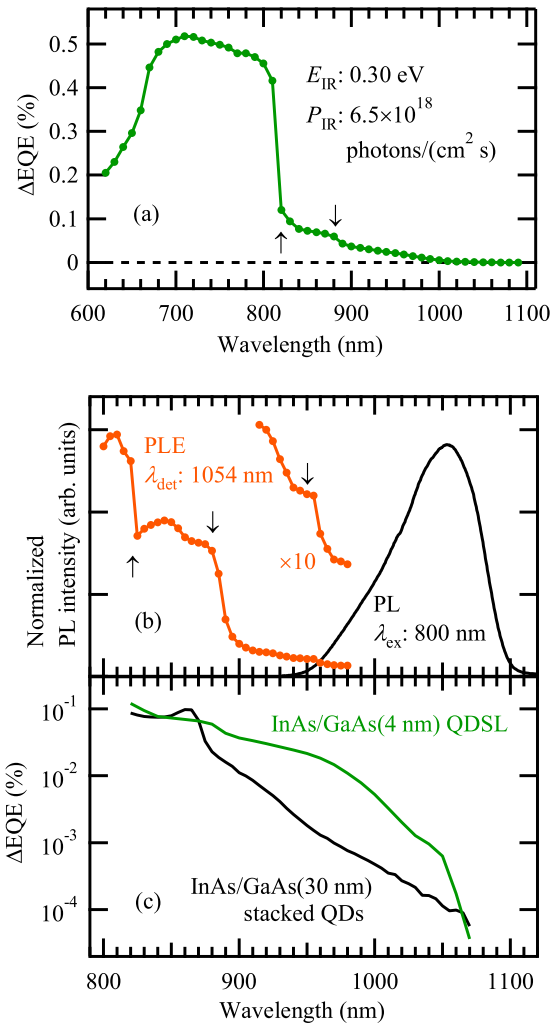

FIG. 2. (Color online) (a) ΔEQE spectrum measured at 9 K. The IR light source used here was a pulsed laser light with a photon energy of 0.30 eV and repetition rate of 200 kHz. The excitation intensity was 6.5×10^{18} photons/(cm^2 s). (b) PL and PLE spectra measured at 9 K. PLE spectrum indicates the PL peak intensity of the fundamental transitions of QDSLs. Several absorption edges are indicated by arrows in the PLE spectrum. (c) Comparison of ΔEQE spectra obtained for InAs/GaAs(4 nm) QDSL and uncoupled InAs/GaAs(30 nm) stacked QDs at 9 K.

large as compared with the result reported in an earlier work done at room temperature [19] because of efficient electron accumulation in the IB of the low internal electric field SC maintained at low temperature. The broad, strong ΔEQE signal appearing in the wavelength region from 700 to 800 nm is attributed to a photocurrent generated by IR photoexcitation of electrons in the IB pumped by the interband transition in GaAs. This indicates that part of the electrons pumped by the interband transition in the GaAs layer are trapped by QDs before being extracted toward the *n*-side electrode. For wavelengths shorter than 700 nm, ΔEQE signal decreases drastically with the wavelength. Because of the shallow penetration depth for the shorter wavelength light, electrons excited in the *p*-layer easily recombine with holes in the VB before drifting toward the QDSLs. As a result, the electron density becomes low in the IB and the IR photoexcitation becomes inefficient. Below the absorption edge of GaAs (820 nm), the ΔEQE spectrum shows a tail structure that arises from the TSPA process. A small edge at approximately 880 nm can be attributed to the absorption edge of the InAs WL. The tail structure of ΔEQE extends further toward the longer wavelength side. These features are consistent with structures observed in a PLE spectrum discussed later. Since the IR excitation power dependence of the ΔEQE signal intensity yields a linear dependence, nonlinear two-photon absorption of the IR photons is negligible in this experiment.

Figure 2(b) shows PL and PLE spectra measured at 9 K. An inhomogeneously broad PL signal appears at 1054 nm, which is attributed to the fundamental transitions of QDSLs. The PLE signal intensity detected at 1054 nm is gradually increases in wavelengths shorter than 1000 nm. The PLE spectrum corresponds to the optical absorption profile. Several absorption edges indicated by arrows were confirmed. The clear edge at 820 nm is due to the GaAs band edge. The edge observed at approximately 880 nm corresponds to absorption of the InAs WL. These two structures were also observed in the ΔEQE spectrum in Fig. 2(a). In the longer wavelength region, a weak absorption edge was found at approximately 950 nm. To clarify the origin of this, we examined the PL peak wavelength as a function of the excitation wavelength. We found that the PL peak starts shifting with the excitation wavelength in the region longer than 950 nm when the inhomogeneously distributed fundamental QDSL states are directly excited as reported in Ref. [24]. The critical wavelength showing the peak shift produced the edge structure at 950 nm in the PLE spectrum. Therefore, this absorption edge located above the inhomogeneously distributed fundamental states can be attributed to the higher excited states of the QDSLs.

Figure 2(c) compares the ΔEQE spectrum obtained for QDSLs of InAs/GaAs(4 nm) with that for uncoupled ten-stacked QDs of InAs/GaAs(30 nm). The thick GaAs spacer layer of 30 nm in the reference SC diminishes the interdot coupling, and miniband is not formed. Hence the comparison shows a clear and significant proof of the SL effect on the SC performance. It is noted that ΔEQE of QDSL is dramatically enhanced in the wavelength region corresponding to the excited states. This is a unique feature appeared in QDSL. ΔEQE is proportional to the intersubband absorption coefficient between IB and CB. The intersubband absorption coefficient is also proportional to the state filling of IB given by the Fermi-Dirac distribution [10]. Next, we discuss influence of carrier dynamics on the state filling.

We measured the excitation power dependence of the PL intensity. The excitation wavelengths, 940, 850, and 780 nm, were chosen to excite the absorption edge at 950 nm, the InAs WL states, and GaAs barrier, respectively. Here, we carefully dealt with the excited carrier density. The carrier densities excited at each wavelength will be different for the same power density because of the different absorption coefficient. According to the PLE spectrum corresponding to the optical absorption profile, we estimated the relative absorption coefficient. Figure 3 shows the integrated intensity of the QDSL fundamental state PL as a function of the excitation power density in the same excited carrier density. The results exhibit different slopes depending on the excitation

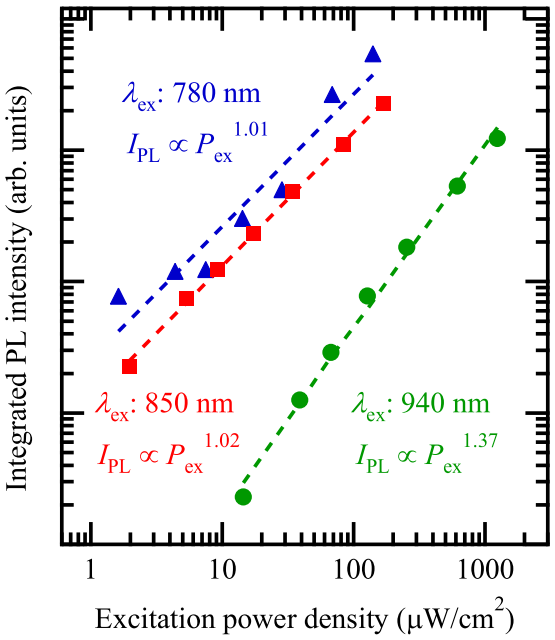

FIG. 3. (Color online) Integrated PL intensity from the fundamental transitions as a function of the excitation power. The excitation wavelengths, 940, 850, and 780 nm, were chosen to excite the absorption edge at 950 nm, the InAs WL states, and GaAs barrier, respectively. Here, the excitation power density was carefully chosen by taking into account the relative absorption coefficient estimated from the PLE spectrum. Dotted lines are fitting of the power dependence.

wavelength. It is noted that the power dependence when selectively exciting the absorption edge at 950 nm demonstrates a superlinear relation, though the slopes for the excitations at the WL and GaAs states were linear. The superlinear dependence indicates that the excited electron and hole are separately relaxing into the QDSL states [25–27]. According to the excitation power dependence of the PL under a higher excitation (not shown here), the first excited states of the QDSLs correspond to the tail structure appeared at the shorter wavelength side (∼1000 nm) of the peak. Thus the energy distribution of the first excited states overlaps with that of the fundamental states. Such energy overlapping will reduce the excitation cross section for the excited states. Thereby, the higher excited states appearing above the inhomogeneously distributed fundamental states play an important role in the efficient spatial carrier separation in the miniband. On the other hand, when excited above the GaAs barrier, the short-wavelength excitations generate carriers dominantly in the thick GaAs layer deposited above (*p*-side) the QDSL layer. Recombination of diffused electrons and holes in QDs causes the linear excitation power dependence as observed at the 780-nm excitation.

When the adjacent QD states along the stacking direction are distributed within the *homogeneous* band, electronic coupling occurs and, thereby, the miniband is formed. The homogeneous linewidth of the excited state resonance is more than one order of magnitude larger than that of the fundamental state resonance because of the weaker electron confinement in the excited state [28]. Such wide homogeneous

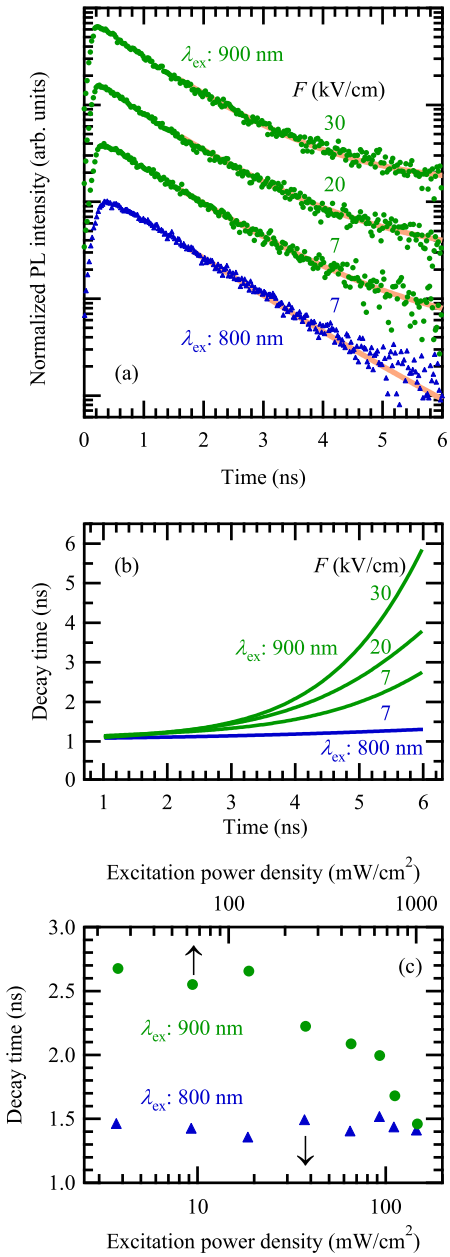

FIG. 4. (Color online) (a) Time-resolved PL intensity from the fundamental transitions. The excitation wavelengths, 900 and 800 nm, were chosen to excite the absorption edge at 950 nm and GaAs barrier, respectively. PL decay curves at different electric fields were measured at the 900-nm excitation. Solid lines indicate best fitting curves, where the coefficients of determination, R^2 values, were 0.936, 0.943, 0.974, and 0.968 for 7 kV/cm at the 800-nm excitation, and 7, 20, and 30 kV/cm at the 900-nm excitation, respectively. (b) Analyzed decay times as a function of the detection-time delay in the stretched exponential decay profile. (c) Excitation power density dependence of the decay time. The excitation power densities were chosen by taking into account the relative absorption coefficient estimated from the PLE spectrum.

linewidth of the excited state easily causes miniband formation even in the inhomogeneous energy distribution along the stacking direction, despite the fact that the miniband is not formed in the fundamental state at the low temperature below

∼20 K. This enables effective carrier transport of electrons and holes in the opposite direction in the miniband of the higher excited states under the influence of the internal electric field. Independent energy relaxation of electrons and holes into the fundamental states located along the stacking direction reduces the recombination rate, causing the electron lifetime to become long, which enhances the chances of intersubband photoexcitation.

To confirm the separate electron-hole energy relaxation we studied the radiative recombination lifetime by the time-resolved PL measurements. Figure 4(a) shows the time-resolved PL intensity from the fundamental transitions. The excitation power densities were 18.5(128) mW/cm^2 for the 800(900)-nm excitation, which was provided to maintain the same excited carrier density. The result of the 800-nm excitation (∼1.55 eV) which is above the GaAs band gap dominantly exhibited a single exponential decay with the decay time of 1.1 ns. The decay time slightly increases with the delay. On the other hand, when excited at 900 nm, this slow decay component turns significant. This slow decay component yields to a stretched exponential profile given by a fractional power law representing a continuous distribution of lifetimes [29]. The solid line in Fig. 4(a) indicates the fitting curve. Figure 4(b) shows analyzed decay times as a function of the detection-time delay. Though the rapid decay component coincides with the decay obtained at the 800-nm excitation, the slow decay component shows the time constant of 2.7 ns at the delay of 6 ns. According to our earlier work [16], the PL decay time of the fundamental state exhibiting the Stark localization under an extremely strong electric field of approximately 200 kV/cm was almost the same as that of conventional single-layer QDs. This is due to the short QD height of approximately 5 nm which negligibly diminishes the spatial carrier separation. Thus this slow decay component can be attributed to recombination of spatially separated electron and hole in the miniband of the excited states. The ΔEQE enhancement in Fig. 2(c) arises from longer carrier lifetime taking over the significant stretched exponential profile. Furthermore, this slow decay component depends on the internal electric field by applying dc bias voltage at 0, −2.6, and −4.6 V for $F = 7$, 20, and 30 kV/cm, respectively. With increasing the electric field, the decay time becomes longer as shown in Fig. 4(b). Since the strong electric field causes significant carrier separation, the slower decay at the higher electric field convincingly supports our discussion.

In addition, we measured the excitation power dependence of the decay time in the same excited carrier density as shown in Fig. 4(c). The decay time excited at 900 nm decreases with the excited carrier density, while one at 800 nm was almost constant. This implies that high density electrons and holes excited by the high-power excitation uniformly occupy the fundamental state of different QDs.

The extension of the electron lifetime reflects on ΔEQE being proportional to the intersubband absorption coefficient determined by the state filling of IB. The slow electron lifetime increases the electron density in IB, which lifts the quasi-Fermi level and increases the filling factor. Thereby, ΔEQE is enhanced. The slower decay component at the 900-nm excitation was approximately 2.1 times longer than that at 800 nm at the delay of 6 ns, which is further extended according to the stretched exponential behavior of the slow decay component. ΔEQE was enhanced approximately 10 times greater at 950 nm by the SL structure. This result indicates that the filling factor changed by the extended electron lifetime remarkably increased the intersubband absorption coefficient. Besides, it is noted that the excitation power density used in the time-resolved measurements is approximately nine orders of magnitude stronger than that used for the EQE measurements, because the electron lifetime decreases with increasing the excitation power density.

In summary, we studied a key mechanism enhancing TSPA in an IBSC that included InAs/GaAs QDSLs. TSPA of subband-gap photons remarkably occurs when pumping electrons from the VB to an absorption edge located above the inhomogeneously distributed fundamental states of QDSLs. The excitation power dependence of the PL intensity and the time-resolved PL demonstrated that electrons and holes separately relax into QDSLs when directly excited at the absorption edge attributed to the higher excited states of the QDSLs. This extends electron lifetime by inhibiting recombination with holes, thereby enhancing the second subband-gap absorption. These results demonstrate an important role of IB electron lifetime in improving the conversion efficiency of IBSCs.

This work has been partially supported by the Incorporated Administrative Agency New Energy and Industrial Technology Development Organization (NEDO), and Ministry of Economy, Trade and Industry (METI), Japan. The authors would like to thank S. Naitoh of the University of Tokyo for fabrication of the reference QD sample.

[1] L. C. Hirst and N. J. Ekins-Daukes, Prog. Photovolt: Res. Appl. **19**, 286 (2011).
[2] W. Shockley and H. J. Queisser, J. Appl. Phys. **32**, 510 (1961).
[3] See http://www.ise.fraunhofer.de/en/press-and-media/press-releases/presseinformationen-2013/world-record-solar-cell-with-44.7-efficiency, for Press Release, Fraunhofer Institute for Solar Energy Systems ISE, 2013, accessed 2014.
[4] A. Luque, J. Appl. Phys. **110**, 031301 (2011).
[5] T. Trupke and P. Würfel, J. Appl. Phys. **96**, 2347 (2004).
[6] T. Kita, *Energy Conversion Efficiency of Solar Cells* (CORONA, Tokyo, 2012), p. 87 (in Japanese).
[7] A. Luque and A. Martí, Phys. Rev. Lett. **78**, 5014 (1997).
[8] A. Luque, A. Martí, and C. Stanley, Nat. Photon. **6**, 146 (2012).
[9] K. Yoshida, Y. Okada, and N. Sano, Appl. Phys. Lett. **97**, 133503 (2010).
[10] W. G. Hu, T. Inoue, O. Kojima, and T. Kita, Appl. Phys. Lett. **97**, 193106 (2010).

[11] A. J. Nozik, Physica E **14**, 115 (2002).
[12] S. Tomić, Phys. Rev. B **82**, 195321 (2010).
[13] K. Nishikawa, Y. Takeda, T. Motohiro, D. Sato, J. Ota, N. Miyashita, and Y. Okada, Appl. Phys. Lett. **100**, 113105 (2012).
[14] A. Takahashi, T. Ueda, Y. Bessho, Y. Harada, T. Kita, E. Taguchi, and H. Yasuda, Phys. Rev. B **87**, 235323 (2013).
[15] Y. Ikeuchi, T. Inoue, M. Asada, Y. Harada, T. Kita, E. Taguchi, and H. Yasuda, Appl. Phys. Express **4**, 062001 (2011).
[16] N. Kasamatsu, T. Kada, A. Hasegawa, Y. Harada, and T. Kita, J. Appl. Phys. **115**, 083510 (2014).
[17] T. Kada, A. Hasegawa, and T. Kita, *2013 JSAP-MRS Joint Symposia*, Kyoto, Japan (unpublished).
[18] A. Martí, E. Antolín, C. R. Stanley, C. D. Farmer, N. López, P. Díaz, E. Cánovas, P. G. Linares, and A. Luque, Phys. Rev. Lett. **97**, 247701 (2006).
[19] Y. Okada, T. Morioka, K. Yoshida, R. Oshima, Y. Shoji, T. Inoue, and T. Kita, J. Appl. Phys. **109**, 024301 (2011).
[20] Y. Shoji, K. Akimoto, and Y. Okada, J. Phys. D: Appl. Phys. **46**, 024002 (2013).
[21] R. Tamaki, Y. Shoji, Y. Okada, and K. Miyano, Appl. Phys. Lett. **105**, 073118 (2014).
[22] S. Asahi, H. Teranishi, N. Kasamatsu, T. Kada, T. Kaizu, and T. Kita, J. Appl. Phys. **116**, 063510 (2014).
[23] E. Antolín, A. Martí, C. D. Farmer, P. G. Linares, E. Hernández, A. M. Sánchez, T. Ben, S. I. Molina, C. R. Stanley, and A. Luque, J. Appl. Phys. **108**, 064513 (2010).
[24] R. Heitz, M. Veit, N. N. Ledentsov, A. Hoffmann, D. Bimberg, V. M. Ustinov, P. S. Kop'ev, and Z. I. Alferov, Phys. Rev. B **56**, 10435 (1997).
[25] T. Kita, R. Hasagawa, and T. Inoue, J. Appl. Phys. **110**, 103511 (2011).
[26] Y. D. Jang, J. Park, D. Lee, D. J. Mowbray, M. S. Skolnick, H. Y. Liu, M. Hopkinson, and R. A. Hogg, Appl. Phys. Lett. **95**, 171902 (2009).
[27] E. C. Le Ru, J. Fack, and R. Murray, Phys. Rev. B **67**, 245318 (2003).
[28] S. Seidl, M. Kroner, C. Lux, A. W. Holleitner, K. Karrai, R. J. Warburton, A. Badolato, and P. M. Petroff, Appl. Phys. Lett. **92**, 153103 (2008).
[29] R. Chen, J. Lumin. **102-103**, 510 (2003).